Structure Development during Shear Flow-Induced Crystallization of i-PP: In-Situ Small-Angle X-ray Scattering Study

Rajesh H. Somani, Benjamin S. Hsiao,* and Aurora Nogales†

Department of Chemistry, State University of New York, Stony Brook, New York 11794-3400

Srivatsan Srinivas and Andy H. Tsou

ExxonMobil Chemical Company, Baytown Polymers Center, Texas 77522

Igors Sics, Francisco J. Balta-Calleja, and Tiberio A. Ezquerra

Instituto de Estructura de la Materia, Madrid, Spain

Received June 27, 2000; Revised Manuscript Received August 30, 2000

ABSTRACT: In-situ synchrotron small-angle X-ray scattering (SAXS) was used to follow orientation-induced crystallization of isotactic polypropylene (i-PP) in the subcooled melt at 140 °C after step shear under isothermal conditions. The melt was subjected to a shear strain of 1428% at three different shear rates (10, 57, and 102 s^{-1}) using a modified Linkam shear stage. The SAXS patterns showed strong meridional reflections due to the rapid development of oriented polymer crystallites within the melt. On the basis of the SAXS data, a schematic representation of nucleation and growth in orientation-induced crystallization of i-PP is proposed. During flow, orientation causes alignment of chain segments of polymer molecules and results in the formation of primary nuclei in the flow direction. These nuclei facilitate the growth of oriented crystal lamellae that align perpendicular to the flow direction. The half-time of crystallization was calculated from the time evolution profiles of the total scattered intensity. The crystallization kinetics was found to increase by 2 orders of magnitude as compared to quiescent crystallization. A method was used to deconvolute the total integrated scattered intensity into contributions arising from the isotropic and anisotropic components of the crystallized chains. The fraction of oriented crystallites was determined from the ratio of the scattered intensity due to the oriented (anisotropic) component to the total scattered intensity. At low shear rates (∼10 s^{-1}) the oriented fraction in the polymer bulk was lower than at high shear rates (57 and 102 s^{-1}). It was shown that only the polymer molecules above a "critical orientation molecular weight" (M^*) could become oriented at a given shear rate ($\dot{\gamma}$). The M^* values at different shear rates were determined from the area fractions of the molecular weight distribution of the polymer. The observed dependence of M^* on shear rate was fit to the relationship $M^* \propto \dot{\gamma}^{-\alpha}$, with α being an exponent. Analysis of results suggests that the value of M^* is sensitive at low shear rates (below 60 s^{-1}) but not at high shear rates. Experimental results are shown to be in agreement with theoretical predictions having the α value of 0.15.

Introduction

In most polymer processing operations, such as extrusion, injection molding, fiber spinning, etc., the molten polymer is exposed to varying levels of flow fields (elongation, shear, mixed).[1] In the 1970s, great efforts were devoted to elucidate the development of the shish-kebab morphology under elongational flow from dilute polymer solutions.[2−6] Subsequently, the shish-kebab formation in polymer melts under elongational flow or high shear flow was object of intense interest.[6−16] Shear flow was often considered a "weak" flow, incapable of providing sufficient extension of polymer chains to induce fibrillar (shish) formation at different stages of the process. However, in polymer melts even shear flow modifies the crystallization behavior and the resulting morphologies; shear flow accelerates, in fact, the overall kinetics,[17−24] and shish-kebab structures have been observed in the deformed polymer matrix.[6,8,9,13,25] A summary of shear-induced crystallization studies has recently been compiled by Tribout.[26]

It is known that polymer melts, under the influence of a shear field (rate and total strain), exhibit an increased rate of crystallization and a different morphology, when compared with the quiescent melts.[6−13] The resultant morphology has been shown to have direct impact on the improved properties. Kalay[27] reported that shear-controlled orientation injection molding (SCORIM) resulted in more pronounced orientation with a substantial increase in Young's modulus of the final products produced. The enhancements in mechanical properties of the SCORIM isotactic polypropylene (i-PP) products were attributed to the shish-kebab morphology developed by the action of shear on the solidifying melt. Furthermore, Huang[28] demonstrated that improved properties in solid-state polypropylene could be produced from continuous melt extrusion under controlled processing conditions. For example, self-reinforced i-PP sheets prepared at 172 °C and a die pressure of 40 MPa exhibited higher values of melting temperature, tensile strength, and light transmittance than when prepared at 162 °C. This was attributed to a more developed oriented extended-chain crystalline structure in the former.

The crystallization process in polymers and the resultant morphology are strongly dependent on parameters such as processing temperature, applied shear (or elongation) rate, and shear strain.[29] Molecular parameters, such as molecular weight, molecular weight

* Author for correspondence.
† Current address: Instituto de Estructura de la Materia, Madrid, Spain.

10.1021/ma001124z CCC: $19.00
Published on Web 11/17/2000

distribution, chain branching, etc., and the presence of nucleating agents also play an important role. The solid-state structure of i-PP reflects very sensitively to any changes in the aforementioned parameters.[30] Several researchers have investigated the effects of shear (and elongation) fields on the crystalline morphology of i-PP. Varga et al.[31] studied shear-induced crystallization of i-PP and its copolymers using a thermo-optical technique and concluded that melt shearing caused the development of row nuclei in the form of microfibrillar bundles. Row nuclei promoted the epitaxial growth of folded chain lamellae that filled the space normal (perpendicular) to the row nuclei, resulting in a supermolecular structure of cylindrical symmetry. This morphology was referred to as a cylindrite by Kargin et al.[32] and Binsbergen.[33]

According to Thomason and Van Rooyen,[34] a low level of applied stress was sufficient to create a shear-induced layer in a Twaron aramid fiber/PP system. These authors observed two distinct morphologies in the melt undergoing shear: bulk spherulites and a shear-induced layer. Misra et al.[35] studied the role of molecular weight distribution on the spinnability, structure, and properties of melt-spun i-PP filaments. Vleeshouwers and Meijer[36] reported the influence of shear on isothermal crystallization of i-PP of different molecular weights and distribution. Shear rate and duration experiments revealed independent influences on crystallization. Short times at high rates were found to be most effective. Furthermore, it was shown that the crystallization behavior was very sensitive to molecular weight and MWD (molecular weight distribution). Moitzi and Skalicky[37] indicated that even a small shearing of the melt for a few seconds enhanced the crystallization of i-PP at 130 and 135 °C. In a recent study Haudin and Monasse[38] measured the crystallization kinetics of polypropylenes of various molecular weights during shear experiments with a fiber-pullout device. They observed that the crystallization sensitivity of a given i-PP to shear depended on its molecular weight.

A quantitative evaluation of shear field effects is, at present, hampered by the difficulty in description of the crystal morphology and molecular conformation of crystals grown from a deformed melt.[39] Very few in-situ measurements are concerned with the nuclei formed under shear and the subsequent lamellar growth.[34] Janeschitz-Kriegl and co-workers[8,9] introduced the method using high shear rate and short-term shearing with both in-situ optical techniques to monitor of the structure development in polymer melts and ex-situ microscopy measurements of the deformed samples. The elegant experiments designed by Janeschitz-Kriegl and co-workers isolated the effect of flow on subsequent structure development. Their experiment essentially eliminated effects of reorientation of crystallites by stopping flow before appreciable crystallization occurred. Kornfield and co-workers[12,13] have recently studied the influence of short-term shearing using *both* in-situ optical (birefringence) and wide-angle X-ray diffraction (WAXD) and ex-situ microscopy techniques. They reported that the i-PP specimens quenched after shear crystallization revealed that highly oriented crystallites developed in a row nucleated or shish-kebab morphology; the lamellae (kebab) grew radially outward from the central line nuclei (shish) until they impinged with each other.

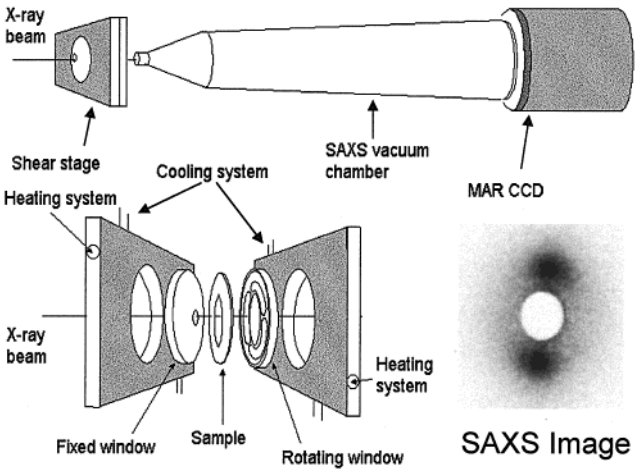

Figure 1. Schematics of the Linkam shear stage, showing the placement of sample and the rotating and stationary plates. The synchrotron small-angle X-ray scattering (SAXS) setup with a 2 D MARCCD detector is also shown.

Step shear deformation experiments on i-PP using small-angle X-ray scattering (SAXS) have not been reported previously in the literature. The aim of the present study is thus to extend the above investigations to examine the structure development of i-PP in undercooled melt (at 140 °C) subjected to a brief impulse of step shear (with high shear rates and high strains), using in-situ synchrotron SAXS. It will be shown that the combination of high shear rate (similar to polymer processing operations) and high strain preferentially orients the polymer molecules in the flow direction. The imposed shear field affects the extent of molecular orientation in the melt and the final resulting crystalline morphology. An attempt to estimate the fraction of oriented species in the bulk polymer is made on the basis of the SAXS data taken at different shear rates. Finally, the concept of "critical orientation molecular weight" (M^*), defining the molecules above a certain chain length that become oriented at a given shear rate, is introduced. The relationship between M^* and the shear rate ($\dot{\gamma}$) has also been explored, as was first proposed by Keller and co-workers.[3−6]

Experimental Section

Materials. Ziegler−Natta isotactic polypropylene (i-PP) homopolymer supplied by ExxonMobil Chemical Company was used in this study. The molecular weights of the i-PP resin, as obtained from the GPC experiments, were M_n = 92 203, M_w = 368 935, and M_z = 964 632. Polymer films of 0.5−1.0 mm thickness were prepared in a laboratory press at 210 °C. Samples in the form of a ring (i.d. = 10 mm, o.d. = 20 mm) were cut from the molded films for the X-ray scattering measurements.

Shear Apparatus. A Linkam CSS-450 high-temperature shearing stage modified for "in-situ" X-ray scattering studies was used to precisely control shear field and thermal history of the polymer samples. Kapton windows were used in place of the standard quartz optical windows on the top and bottom steel blocks (two parallel plates) of the Linkam stage (Figure 1). The sample was held in the gap between the two windows and was sheared by rotating the bottom plate by a precision stepping motor, while the top plate remained stationary. The top plate had a narrow aperture hole (diameter = 3 mm), which allowed the X-ray beam (diameter = 0.9 mm) to enter the sample. The bottom plate had three open slots (wider than the hole in the top window), which allowed the scattered X-ray beam to pass directly through the sheared sample. The windows fit together in such a way that the sample was sealed.

Polymer melts were fairly viscous, and no leakage was detected even when the Linkam stage was mounted in the vertical position (necessary since the X-ray beam travels horizontally). The mechanical design and electronics of the Linkam stage provided a precise control of various parameters of the shear experiment, which included temperature, heating/cooling rates, sample thickness, shear rate, and shear strain (shear duration) as well as shear mode—step, steady, and oscillatory. The shearing stage was compact and could be easily set up for in-situ X-ray scattering/diffraction experiments in a synchrotron beamline.

In all our experiments, the step shear mode was selected. The shear rate and strain conditions were chosen in such a way that the bottom window would rotate less than one full circle (360°). The advantage of the step shear mode is that the polymer melt is deformed only once, as compared to constant-rate shear, in which the fluid elements rotate as well as undergo shear. The strain rate will change sign periodically in the constant-rate shear.[39] The total strain and the strain rate cannot be varied independently in constant-rate shear flow, and experiments cannot be conclusive as to whether strain rate or total strain governs the onset of orientation-induced crystallization in flowing melts. Keller and Kolnaar[6] pointed out the need for an experimental setup where the strain rate and the total strain could be varied independently. The step shear mode in the Linkam shear stage provided such a setup, in which the shear parameters (shear rate and percent strain) were varied independently. The Linkam apparatus offered a parallel-plate shearing geometry. In this instrument, the step shear was applied by rotating the bottom plate at an angular velocity ω (corresponding to the desired shear rate $\dot{\gamma} = r\omega/d$, where r is the radius and d is the sample thickness) through an angle ϕ (corresponding to the desired strain $\gamma = r\phi/d$), while the top plate remains stationary. Since velocity gradient is constant across the thickness of the sample, both the shear rate and the shear strain at any point across the thickness are also constant.

Small-Angle X-ray Scattering. SAXS measurements were carried out at the Advanced Polymers Beamline (X27C, λ = 1.307 Å) in the National Synchrotron Light Source (NSLS), Brookhaven National Laboratory (BNL). A three-pinhole collimator system was used for beam alignment.[40] A 2D MAR CCD X-ray detector (MARUSA) was employed for the detection of 2D SAXS images, having a resolution of 512 × 512 pixels (pixel size = 257.6 μm). The sample to detector distance was 1740 mm. The schematic illustrating the SAXS setup is presented in Figure 1.

Experimental Procedure. In each experiment, the polymer sample (in the form of a ring) was mounted between the two X-ray windows. The gap between the two windows was set equal to the sample thickness. To ensure that the polymer melt was free of any memory effects associated with clusters, crystal aggregates, and molecular conformation due to temperature and deformation history, all samples were subjected to the same thermal history, as shown in Figure 2. The temperature protocol and shear conditions used during the SAXS experiments are shown in Figure 2. The experimental temperature profiles were set as follows: (1) heating at a rate of 10 °C/min from room temperature to 210 °C; (2) holding the temperature at 210 °C for 5 min to eliminate residual structure; (3) cooling at a rate of 30 °C/min down to 140 °C; (4) holding the temperature at 140 °C for 30 min for X-ray measurements.

A crystallization temperature of 140 °C was chosen so that the nucleation and crystal growth times were relatively long under quiescent conditions. The half-time of crystallization under quiescent conditions for i-PP at this temperature was $\sim 10^4$ s,[31] which had also been confirmed in our laboratory. Hence, the observed changes in the crystallization kinetics at 140 °C after shear could be attributed solely to the imposed shear conditions.

Two-dimensional SAXS images were taken immediately after the polymer reached 140 °C. The data acquisition time for each scattering pattern (image) was 10 s, with an interval of 5 s between adjacent images. Typically 100 SAXS images were collected in a single run. After collection of three images where no shear was present, the polymer melt was subjected to a brief impulse of step shear from time $t = 0$ to t_s (Figure 2). The step shear conditions were also monitored by a video CCD camera. Three different shear rates, 10, 57, and 102 s^{-1} were used. A high strain value of 1428% was used in all our experiments. Thus, the duration of the step shear was 1.4, 0.25, and 0.14 s, corresponding to the shear rates of 10, 57, and 102 s^{-1}, respectively. The SAXS images were collected continuously: before, during, and after cessation of the applied shear. The scattering images represented the average of the scattered intensity from the scatterers across the thickness of the sample.

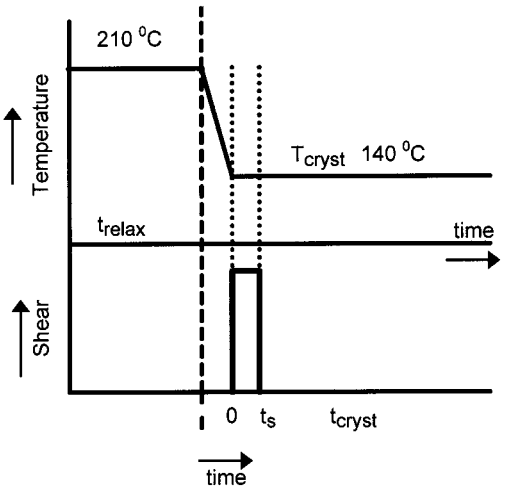

Figure 2. Schematics of the temperature and shear conditions as a function of time during step shear SAXS experiments.

An air scattering pattern (10 s acquisition time) at a temperature of 140 °C with no sample between the two windows of the shear stage was also collected. The air scattering pattern was used for background correction of the scattering data; X-ray data were also normalized for sample thickness. Subsequent analysis of the X-ray data was carried out using the corrected and normalized scattering patterns.

Transmission Electron Microscopy. After the SAXS experiment, i-PP samples were cooled to room temperature and the crystalline structures in the sample were observed using a transmission electron microscope (TEM). Each sample was cryofaced at −130 °C and then stained with Montecino's stain for 3 h. Stained sections were taken from the sample faces by ambient cryotomy and imaged by a JEOL 2000FX TEM at 160 kV.

Results

SAXS Patterns. Figure 3 illustrates a representative series of two-dimensional SAXS patterns of the i-PP sample at 140 °C before and after application of a step shear (102 s^{-1} shear rate and 1428% strain). The pattern of the initial amorphous melt (Figure 3a) consists of a very weak diffuse scattering profile from the isotropic melt, indicating the absence of any detectable structures and/or preferred orientation. This pattern is observed before shear in all experiments, confirming thermal clearing of all residual structures in the i-PP melt.

Figure 3b shows the scattering pattern obtained 120 s after the applied shear (duration of shear was 0.14 s). The pattern clearly shows the appearance of meridional maxima from the oriented scatterers (growing lamellae in the melt). It should be emphasized that discrete reflections were observed almost immediately after the shear pulse was applied. The data acquisition time for each image was 10 s, and even the first image collected

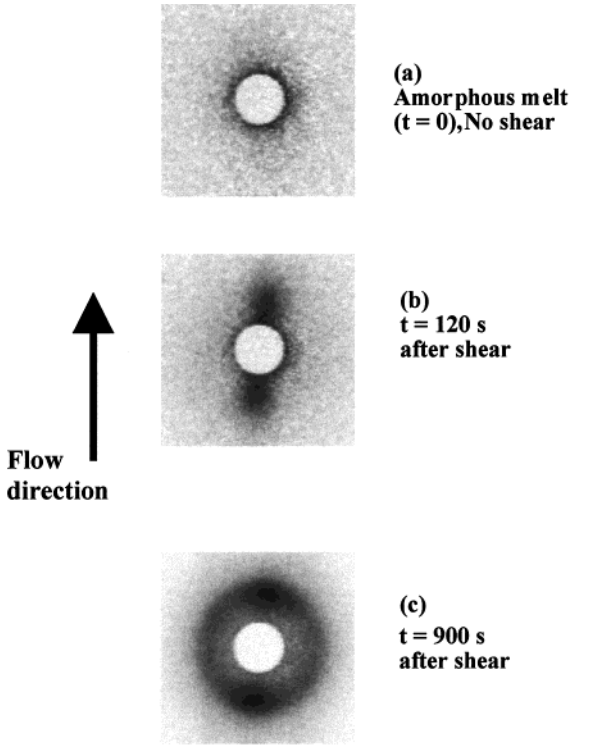

Figure 3. SAXS patterns of i-PP at 140 °C before and after step shear (shear rate = 102 s^{-1}, strain = 1428%): (a) image of amorphous melt before shear, (b) image obtained 120 s after cessation of shear, and (c) image obtained 900 s after cessation of shear. (The flow direction in the sheared melt is not strictly vertical, but it is tangential to the rotating movement of the bottom plate. This gives a slightly angular tilt to the meridional reflections on the SAXS patterns.)

after shear shows discrete reflections. Thus, oriented structures clearly develop immediately after application of the brief pulse of the step shear. The meridional maxima imply that the packages or stacks of crystal lamellae have already formed in the crystallizing polymer melt. The intensity of discrete reflections in the consecutive images gradually becomes stronger, due to growth of lamellar structures in the melt. Furthermore, the azimuthal width becomes broader, owing to a decrease in orientation of the lamellar structures. After a certain time, the intensity of the discrete reflections remained constant, and no significant change was observed anymore in the scattering patterns. Figure 3c shows the scattering pattern of the sample 900 s after the applied shear. Here, the oriented SAXS maxima are better defined, though they are superimposed on an strong isotropic scattering ring. Note that no equatorial reflections are seen in the SAXS patterns, which indicates that the extended chain crystals (the shish structure) are not present, although it is possible that they are farther apart that they cannot be observed in SAXS. (The maximum spatial resolution of this setup is 1000 Å.)

A TEM micrograph of the crystallized polymer sectioned film (after the SAXS experiment) is shown in Figure 4. The TEM micrograph clearly shows the oriented lamellar stacks in perpendicular to the flow direction; however, it does not show presence of the extended chain crystals (shish). Both the SAXS and TEM observations indicate no evidence of the shish structures under our experimental conditions. Interpretations of these observations are given in the Discussion section.

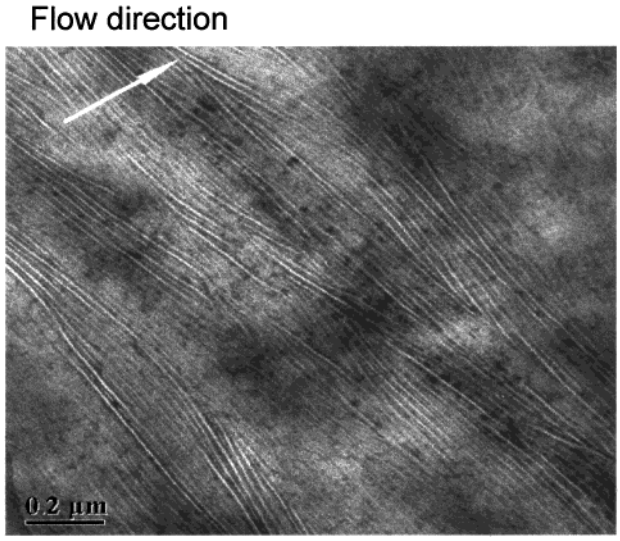

Figure 4. A typical transmission electron micrograph of the sectioned polymer sample after SAXS experiment (shear rate = 102 s^{-1}, strain = 1428%).

Analysis of SAXS Data. In each experiment, at least 100 SAXS patterns were collected, starting with the completely amorphous melt at 140 °C (before shear), during shear, and after cessation of shear. The time period between each image was 15 s. The SAXS image at time $t = 0$ corresponds to the amorphous melt. In all experiments, the SAXS image at $t = 15$ s shows the discrete reflections (although weaker in intensity) due to the growth of the oriented crystalline lamellae in the melt. The sheared melt crystallizes completely, in a few minutes, as evidenced by the fact that there is no change in the SAXS pattern thereafter.

The total (or integrated) scattered intensity of each SAXS pattern is due to the contribution of all the scatterers in the polymer sample. Initially, at $t = 0$, there are very few scattering species (or scatterers) in the polymer melt, and the integrated intensity is, consequently, low. Owing to the imposed step shear, the chain segments of polymer molecules align in the flow direction and form "orientation-induced nuclei" via primary nucleation (initiated from a single phase). These nuclei provide the nucleating sites for the crystallites that grow (via secondary nucleation) after cessation of shear. However, it has been reported that the lamellar thickness, crosshatching frequencies, and growth rates are independent of the type of nucleation: point, surface, or row nucleated.[41] Thus, the growth of both the oriented crystallites and the randomly distributed crystallites is expected to occur in the melt after cessation of shear. We expect the resultant morphology of the polymer bulk to consist of both the preferentially oriented crystalline lamellae and the randomly distributed lamellae.

The total scattered intensity, ($I_{total}[s,\phi]$), from the polymer sample thus can be deconvoluted into two components,[1] $I_{unoriented}[s]$, which is due to scattering from the randomly distributed crystalline lamellae, and[2] $I_{oriented}[s,\phi]$, originated by scattering from the oriented lamellae. The total scattered intensity is represented as follows:

$$I_{total}[s,\phi] = I_{unoriented}[s] + I_{oriented}[s,\phi] \qquad (1)$$

where $s = 2 \sin \theta/\lambda$ is the scattering vector, 2θ is the scattering angle, and ϕ is the azimuthal angle. The

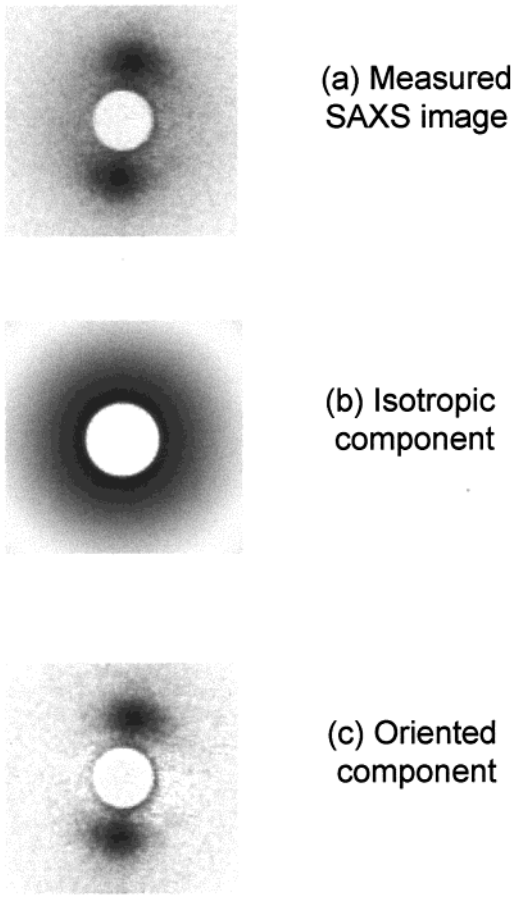

Figure 5. Deconvolution procedure of the scattering into contributions from the oriented scatterers and from the unoriented scatterers: (a) original SAXS image, (b) intensity pattern of the isotropic scatterers (obtained from custom method described in the text, the shown intensity was normalized to a different scale than (a) and (c)), (c) intensity pattern of the oriented scatterers (from image a minus image b).

scattering from the unoriented component also includes the Compton scattering from the chemical structure, which is small (especially at low angles) and may be ignored. The isotropic component of the total intensity, $I_{\text{unoriented}}$, was obtained from the custom method.[42] In brief, a series of the azimuthal scans were drawn along the scattering vector starting from the center of the diffraction pattern. At each scattering angle, 2θ, a minimum scattering intensity value was determined from the corresponding azimuthal scan. Thus, a series of minimum scattering intensity values were obtained from the azimuthal scans at each scattering angle. This minimum intensity was then attributed to the isotropic scatterers, and deviations in the intensity along the azimuth were attributed to the presence of preferentially oriented scatterers. The intensity envelope obtained from the series of minimum values represented a contribution from the unoriented scatterers. We note that this method is prone to error if the signal-to-noise ratio is low or the data consist of low valued points (such as defective pixels on the detector). The unoriented intensity envelope, however, can be extrapolated by curve fitting of the minimum intensity values to minimize these effects.

The analytical procedure is further explained in Figure 5, showing a 2D SAXS image of the total scattered intensity pattern (a frame 300 s after shear is shown in the example, Figure 5a). Figure 5b shows

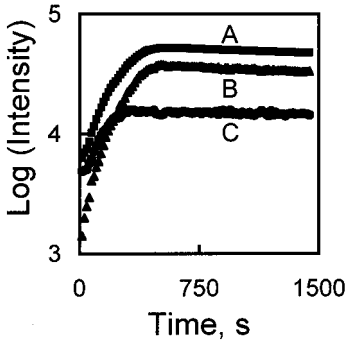

Figure 6. Time evolution of (A) total scattered intensity, (B) scattered intensity from the unoriented scatterers, and (C) scattered intensity from the oriented scatterers after the step shear (rate = 102 s^{-1}, strain = 1428%, T = 140 °C).

the 2D image of the isotropic intensity pattern determined from the above method. The pattern clearly shows a ring with scattering maximum, similar to the scattering pattern of crystallites in an isotropic sample. Figure 5c shows the 2D image obtained after subtraction of the image corresponding to the isotropic component from the total scattered intensity image (image b subtracted from image a). The strong scattering peaks on the meridian from the oriented scatterers can be clearly seen in Figure 5c.

The time evolution of the total scattered intensity, the azimuthal independent component, and the intensity due to the oriented scatterers are presented in Figure 6. The total scattering intensity rises very rapidly after the application of the shear pulse; nearly a sudden intensity increase can be clearly seen in curve A. The total integrated intensity reaches a plateau shortly thereafter, indicating completion of crystallization. The azimuthal independent component of the total scattered intensity (curve B) has a low initial value (as one would expect due to the absence of the random scatterers) and, therefore, a very small contribution to the total scattered intensity at time equal to zero. As the randomly distributed crystallites grow in the melt, the scattered intensity increases and, as in the case of total scattered intensity curve, reaches a steady state value at the end of crystallization. On the other hand, the scattered intensity ascribed to the oriented crystallites has a higher contribution to the total scattered intensity in the beginning, that is, immediately after shear (curve C). The contribution of the oriented component increases as the oriented crystals grow and reaches a steady value at the end of crystallization, as in the other two cases (curves A and B). It should be noted that the scattering from the oriented crystallites reaches a plateau before the scattering from the unoriented crystallites.

Typical time evolution profiles of the long period values (L_B) during shear relaxation (shear rate = 57 s^{-1}, T = 140 °C, strain = 1428%), determined from the scattering maximum along the equator and the meridian by using Bragg's law, are shown in Figure 7. The long period value along the meridian represents the average spacing of the orientated lamellae, and the long period along the equator represents the average spacing of the unoriented crystallites. It is seen that the average long period from the orientated crystallites is generally larger than that of the unoriented crystallites. In addition, this long period decreases rapidly with time in the initial stages of crystallization. At the later stages, both long period values (oriented and unoriented crystallites) are seen to decrease at a similar but lower rate.

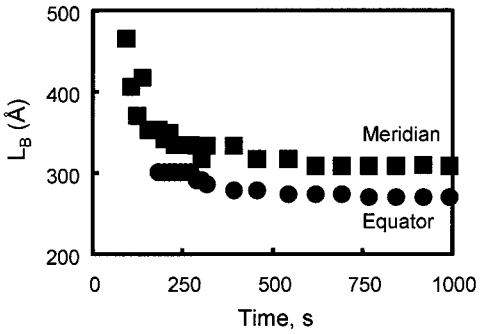

Figure 7. Typical time evolution profiles of the long periods along the equator (representing the unoriented crystallites) and the meridian (representing the oriented crystallites) (shear rate = 57 s^{-1}, T = 140 °C, strain = 1428%).

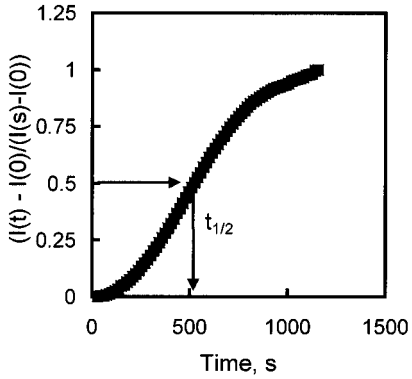

Figure 8. Crystallization kinetics (estimated from the total scattered intensity versus time) of i-PP at 140 °C after the step shear ($t_{1/2}$ is the half-time of crystallization).

Half-Time of Crystallization. The half-time of crystallization for isotactic polypropylene at 140 °C under different shear rates (10, 57, and 102 s^{-1}) was determined from the total scattered intensity profiles. At $t = 0$, the value of the total scattered intensity, $I(0)$, is due to the amorphous, noncrystalline melt. The increase in total scattered intensity, $I(t) - I(0)$, is then directly proportional to the growth of the crystallites in the polymer. The total scattered intensity reaches a plateau, $I(s)$ (steady-state value), at the end of crystallization. The fraction of crystallized material, X_c, can be approximated as

$$X_c = [I(t) - I(0)]/[I(s) - I(0)] \qquad (2)$$

Figure 8 shows the time evolution profile of X_c for the i-PP sample at 140 °C after application of the step shear using a shear rate of 10 s^{-1} and 1428% strain. The half-time of crystallization was taken as the time corresponding to $X_c = 0.5$. The half-time of crystallization for the i-PP sample under these conditions was found to be 525 s.

Effect of Shear Rate. Shear rate is, obviously, one of the most important parameters in the shear-induced crystallization of polymer melts. The shear rate (and shear stress) must be high enough to orient and align the polymer chains in the melt to form stable nuclei in the flow direction. The stability of the orientation-induced structures formed after the application of the shear fields depends on relaxation behaviors of the polymer chains in the melt. The relaxation behavior of polymer molecules is primarily dependent on the chain length (molecular weight) and temperature. It has been shown[8] that the temperature dependence of the relaxation time is much stronger than of zero shear viscosity. Hence, under isothermal conditions, the molecular weight is expected to play a major role in governing stability of the oriented structures after cessation of shear. Longer chain molecules take a longer time to relax from deformation than shorter ones and thus have a better chance of being oriented. In polymers with broad molecular weight distributions (chain lengths), the longer chains from the high molecular weight tail would be more likely to give rise to orientation-induced nuclei due to higher degree of orientation compared to the case of shorter chains. The short chain molecules relax in a very short time after deformation and hence cannot easily form nuclei under flow. The extent of orientation of the polymer molecules, and stability of the resulting orientation-induced nuclei, depend on both the level of the deformation (strain) and the deformation rate (shear rate or elongation rate) relative to the relaxation rate of the molecules. At low strains (even at high shear rates) the orientation and alignment of polymer chains are not sufficient to form nuclei. At low shear rates (and even at high strains), the oriented chains have sufficient time to relax, and stable nuclei cannot be formed. Thus, at a given strain, the oriented fraction in the polymer crystallized after deformation is expected to be higher at high shear rates than the values at low shear rates. As shown earlier, the crystallization time after deformation is strongly influenced by the enhanced nucleation and the growth of the crystallites. Figure 9 illustrates the effect of shear rate on both the oriented fraction and the half-time of crystallization for the i-PP sample at 140 °C. As expected, at low shear rates (10 s^{-1}), the oriented fraction is lower than that at high shear rates (57 and 102 s^{-1}). Also, the corresponding half-times of crystallization are longer than that at high shear rates (57 and 102 s^{-1}). It should be noted that these crystallization half-times are still much lower (525 s at 10 s^{-1}) than that of quiescent crystallization ($\sim 10^4$ s) by about 2 orders of magnitude. Interestingly, the data from Figure 9 revealed that the oriented fraction and the half-time of crystallization do not show significant changes when the shear rate is increased from 57 to 102 s^{-1}.

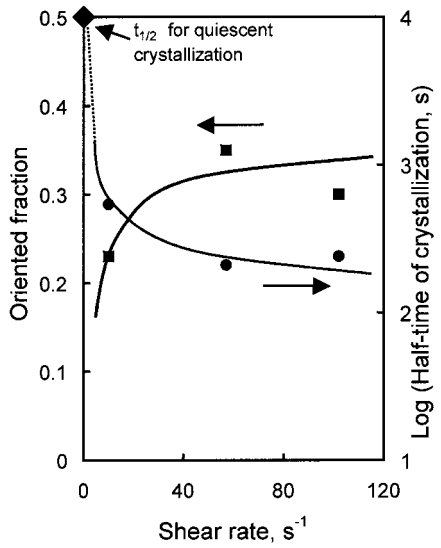

Figure 9. Fraction of oriented material and half-time of crystallization as a function of shear rate (at constant strain = 1428%) in i-PP at 140 °C.

Discussion

Structure Development. The discrete meridional reflections in the SAXS patterns (along the shear direction) can be ascribed to the periodic arrangement of the crystal lamellae perpendicular to the flow direction (the kebab structure). Application of Bragg's equation to the discrete reflections leads to the long spacing L, whereas the intensity distribution is a product of lamellar population, orientation, and density contrast between the crystal and amorphous phases. The intensity and azimuthal breadth of scattering peaks are a measure of the number and orientation of scatterers in the polymer sample.

The intensity of the discrete reflections observed in the SAXS pattern after cessation of step shear is strong in the meridian of the pattern (vertical), indicative of the preferential orientation of scatterers (crystal lamellae) perpendicular to the flow direction. Under the conditions used for the SAXS experiment, a diffuse equatorial streak has not been observed in the SAXS pattern. Also, the transmission electron micrographs do not show the extended chain crystal (shish) structure. Based on these observations, the nature of the structure development in i-PP, under the present step shear conditions, is given below.

It is generally known that, upon application of the shear, the polymer molecules in the melt extend in the direction of shear field and form extended microfibrillar structures. It is also widely believed that melt shearing causes the development of row nuclei in the form of microfibrillar bundles,[8,9,12,13,43] which promote the epitaxial growth of folded chain lamellae that filled the space normal (perpendicular) to the row nuclei, resulting in a supermolecular morphological structure known as shish-kebab. Although we do not dispute the formation of shish-kebab structures in shear flow, the resultant morphology is certainly expected to be dependent on the particular experimental conditions. Under the present experimental conditions, there is no direct evidence of the presence of the extended chain structures (shish). Both SAXS data and TEM micrographs do not show any evidence of the presence of these structures. Even if present, they are very far apart and few in number. (We acknowledge that a spatial distance of 1000 Å is the detection limit of our SAXS instrument.) On the other hand, the SAXS data clearly show that the oriented crystals (kebabs) grow immediately after the application of shear (t < 15 s). Our interpretation of these results is as follows. Shear induces orientation of the polymer molecules in the flow direction. Alignment of the chain segments of polymer molecules is a natural consequence of this process. At a given temperature and external field conditions, the degree of orientation from the initial random coil conformation and the extent of their alignment will, obviously, vary depending on molecular weight, relaxation time, etc. Hence, it is possible that, under certain experimental conditions, only some of the chain segments of the molecule are oriented in the flow direction, and the other segments, especially those near the chain ends, remain unoriented (or have random orientation with respect to flow direction). A cluster of aligned chain segments can form under these conditions, and this cluster can further initiate a primary nucleus assuming that the helical arrangement of the bundled i-PP chains segments is correct. (Note that i-PP chains have four types of helical hands: left- and right-handed helices as well as "up" and "down" helices concerning the pending CH_3 group; the helical arrangement is very specific in the α-monoclinic unit cell structure.[44]) The oriented crystals originate from the shear-induced primary nuclei and grow by the process of secondary nucleation (involving two phases). The tiny primary nuclei, difficult to be identified by SAXS or TEM, are responsible for the growth of the oriented crystals. The formation of extended chain crystal (row nuclei or shish) is not required for the initiation of these kebab-like crystals. We would like to add that it is entirely likely that the growth of the primary nucleus in the flow direction (by increased alignment of the remaining chain segments) can also lead to formation of the long, extended chain crystals or the shish structures, or the microfibrils, if the molecular orientation is high in the vicinity. The meridional reflections observed in the SAXS patterns immediately after the brief pulse of the step shear are, hence, due to the instantaneous formation of the primary nuclei and subsequent growth of the lamellae oriented perpendicular to the flow direction.

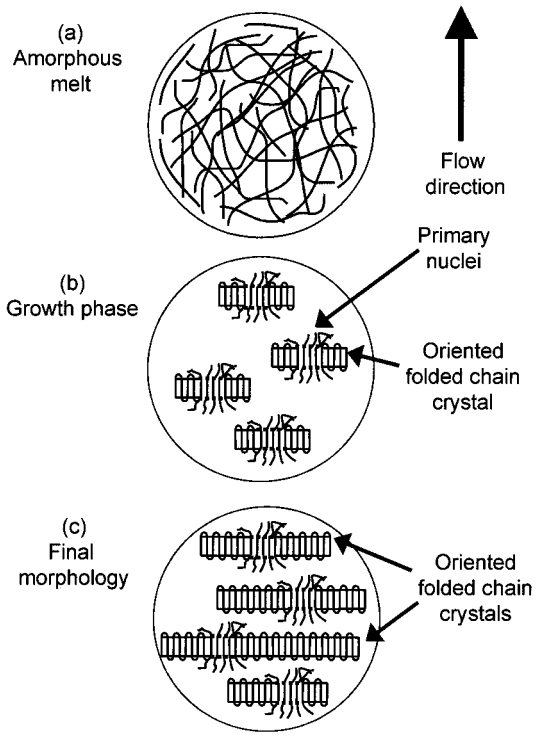

Figure 10. Schematics of the nature of shear-induced primary nuclei and subsequent growth of oriented crystals at the surface undergoing maximum orientation in the step-shear experiment: (a) before shear (amorphous melt, no orientation), (b) at short time (<100 s) after the step shear (primary nuclei and initial growth of the oriented crystals), and (c) final morphology after the step shear (stacks of oriented crystals, kebabs).

On the basis of our observations of the SAXS patterns, TEM micrograph, and the foregoing discussion, a microstructural model for the nature of the primary nuclei and the growth of the oriented crystals after step shear is depicted in Figure 10. The schematics in Figure 10 depict only the event of primary nuclei induced by shear and the subsequent growth of oriented crystals is illustrated in this figure; the unoriented crystals (which are undoubtedly present) are not shown for the sake of clarity. Figure 10a schematically illustrates the random distribution of polymer molecules in the melt in random conformations before shear. Figure 10b showing a

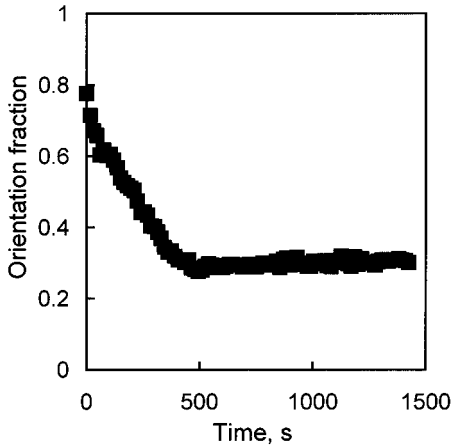

Figure 11. Profile of the development of the oriented fraction in the material as a function of time after the step shear (rate = 102 s^{-1}, strain = 1428%).

"bundle" of aligned chain segments of molecules oriented in the flow direction represents the shear-induced primary nuclei after step shear. Oriented folded chain lamellae (kebabs) grow radially outward in the perpendicular direction to the microfibril axis. The oriented lamellae are depicted farther apart at the beginning to indicate a large value of long spacing, which then decreases as new lamella grow from the other nuclei. Crystallization proceeds by means of further growth and insertion of oriented crystalline lamellae in the bulk of the polymer melt. Figure 10c schematically depicts the oriented crystal morphology in the fully crystallized polymer showing the stacks of lamellae in perpendicular to the flow direction, which is similar to the TEM image seen in Figure 4.

Fraction and Long Period of Oriented Crystallites. Let us assume, in what follows, that the azimuthally dependent ($I_{oriented}[s,\phi]$) component of the total scattered intensity is directly proportional to the oriented fraction (correlated kebabs, with only a little contribution from uncorrelated shish, if present) of the material in polymer matrix. In this case, we ignore the question of the degree of orientation but only address the issue of the fraction of scatterers that are oriented. On the basis of the assumptions above, we can calculate the oriented fraction in the polymer material from the integrated scattered intensity values. The oriented fraction can be defined as the ratio of the scattered intensity due to oriented scatterers to the total scattered intensity. Figure 11 shows the calculated values of the oriented fraction as a function of time for the isotactic polypropylene sample at 140 °C, before and after the application of step shear (102 s^{-1} shear rate and 1428% strain). In the ideal case, before shear there are zero oriented scatterers in the polymer melt. The crystallites grow immediately after shear. These are primarily the oriented lamellae that form due to the applied shear. The rest of the polymer has limited crystallinity (scatterers), and hence, the contribution of the unoriented scatterers to the total intensity is rather small, and the fraction of oriented material immediately after shear is, therefore, very large. As crystallization progresses, the number of unoriented scatterers increases, and the fraction of the unoriented species, as well as its contribution to the total scattered intensity, increase more rapidly than the oriented species. Therefore, the oriented fraction decreases with time after cessation of shear and reaches a steady value. The value of the oriented fraction in the i-PP sample after application of step shear (102 s^{-1} shear rate and 1428% strain) at 140 °C is about 30%. It is interesting to see that the crystallization kinetics of the unoriented species (crystals) under flow are also 2 orders of magnitude faster than those of the polymer at quiescent state. Our recent in-situ WAXD study indicates that the unoriented crystallites formed during flow are primarily in the β form, which are related to the growth of the relaxed and unoriented chains initiated from the surface of the oriented lamellar stack (α form) morphologies. This subject will be discussed in detail elsewhere.

The rapid decrease of the average long period of the oriented crystallites (L_B along the meridian in Figure 7) in the initial stages of crystallization resembles the typical behavior of the long period decrease during isothermal crystallization of semicrystalline polymers under quiescent conditions.[45] This large decrease can be explained by the insertion of new lamellar within the assembly of oriented lamellar stacks. It is conceivable that the initially formed lamellar stacks are loose. As time increases, new lamellae are formed within the stacks, resulting in a sharp reduction of the average long period. The slower decreases in the long periods from both oriented and unoriented crystallites at the later stages are probably due to the production of thinner and defective lamellae. This process has also been widely observed in isothermal quiescent crystallization of typical polymers, which is the characteristics of the "secondary crystallization".[45]

Critical Orientation Molecular Weight. The shear rate effect on the crystallization half-time can be explained if one considers the mechanism of orientation-induced crystallization at a molecular level. A major factor governing the overall dynamics of polymer molecules in the melt under shear is the influence of relaxation behavior of polymer chains. For orientation-induced crystallization, a certain degree of molecular extension must be achieved to induce formation of stable primary nuclei. Both a minimum strain and strain rate values have to be imposed for shear flow to induce crystallization. Thus, a critical shear strain (at constant shear rate) or a critical shear rate (at a constant shear strain) is a precondition for these effects to occur. Note that the shear-induced crystallization effects are found to be critically dependent on temperature and molecular weight (M),[32] with a higher M requiring a lower induction time and, hence, a fluid strain. Also, the critical shear rate for accelerated crystallization shifts to a lower value as molecular weight increases. This is due to the underlying molecular relaxation processes. Keller and co-workers[3-6] have proposed the following relationship in the case of elongational flow induced crystallization:

$$\dot{\epsilon}_c \propto M^{-\beta} \tag{3}$$

where $\dot{\epsilon}_c$ is the critical elongational rate, M is the critical molecular weight (different from the term usually used in rheological studies), and β is a factor that was found to be equal to 1.5 in their experiments with polyethylene solutions. The critical elongation rate is associated with the coil to extended chain transition of the polymer molecules under flow.

Following Keller's observations in elongational flow experiments, we propose similar behavior to explain the results of our shear flow-induced crystallization experi-

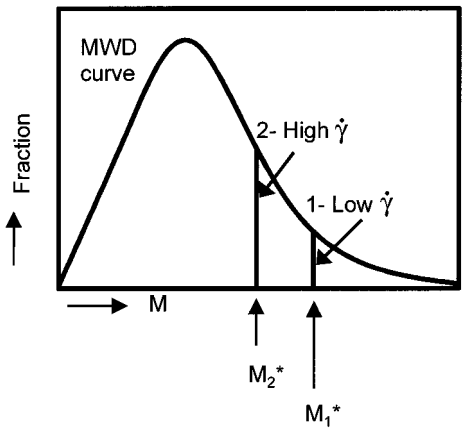

Figure 12. Schematics showing the effect of imposed shear conditions (high and low shear rate) on the shift in the location of the critical orientation molecular weight *M**.

ments. At a given shear rate, only those molecules having a chain length (molecular weight) above a critical value (*critical orientation molecular weight*, we choose this terminology to differentiate it with the term *critical molecular weight* used in rheology) can form stable oriented row nuclei. When the polymer melt, containing a broad chain length distribution, is subjected to a shear flow field of a particular $\dot{\gamma}$, only the longer chains will be oriented (although with different degrees of extension) with a low end cutoff at the critical orientation molecular weight (*M**), while the rest of the molecules will remain unstretched. The result is a bimodal distribution of chain molecules represented by a dual population of oriented and unoriented chains. Increasing $\dot{\gamma}$ does not increase the chain extension substantially but increases the amount of material that becomes oriented by increasingly "cutting into" the distribution from the high molecular tail downward (see Figure 12). A typical MWD curve for a polymeric material is shown in Figure 12. The "critical orientation molecular weight" (*M**) on the curve shifts to a higher value at low deformation rates as shown by lines 1 (low $\dot{\gamma}$) and 2 (high $\dot{\gamma}$). The area under the MWD curve represents the fraction of material above or below the critical orientation molecular weight. If we assume the following relationship between *M** and $\dot{\gamma}$ exists:

$$M^* = K\dot{\gamma}^{-\alpha} \tag{4}$$

$$F(\dot{\gamma}) = M^*/K = \dot{\gamma}^{-\alpha} \tag{5}$$

where *M** is the critical orientation molecular weight, $\dot{\gamma}$ is the shear rate, *K* is a proportionality constant, and α is the exponent (α should be proportional to $1/\beta$ in the Keller equation). The value of α is not known; however, we can examine the nature of the *M** versus $\dot{\gamma}$ variation for various values of α. Figure 13 shows the calculated profiles of the function $F(\dot{\gamma})$ (eq 5) for several values of α. From the curves in Figure 13, it is seen that the value of *M** is more sensitive at low shear rates than at high shear rates, reaching a plateau at high shear rates.

The calculated values of the oriented fraction after deformation and subsequent crystallization can be assumed to be proportional to the fraction of the MWD above the critical orientation molecular weight. The critical orientation molecular weight values corresponding to each shear rate were determined from the GPC

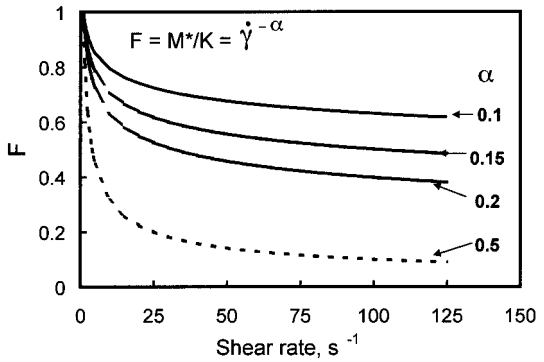

Figure 13. Calculated profiles showing the dependence of the critical orientation molecular weight *M** on shear rate $\dot{\gamma}$ for various values of the exponent α in eq 5.

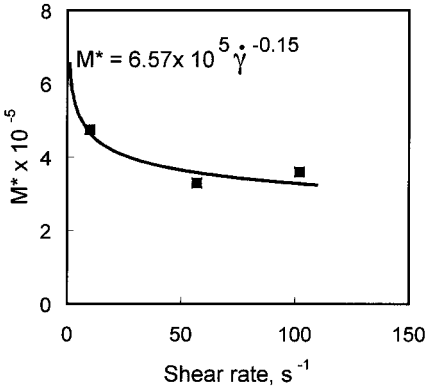

Figure 14. Critical orientation molecular weight *M** (calculated from the observed oriented fraction values from SAXS and the GPC data for the i-PP sample) as a function of shear rate $\dot{\gamma}$ under the step shear (and 1428% strain) at 140 °C (the solid line is the regression fit of the experimental data).

chromatogram for the i-PP resin, and the calculated values of the oriented fraction for various shear rates were determined by SAXS. Figure 14 shows the estimated *M** values for the three shear rates studied. The values of the parameters *K* (=657 000 g/mol) and α (=0.15) in eq 4 were obtained by fitting the experimental data. According to Figure 14, the critical orientation molecular weight, *M** (~300 000 g/mol), does not vary significantly above a shear rate of 60 s^{-1}. Analysis of the experimental data using eq 4 explains why no significant variation in the oriented fraction was observed at shear rates of 57 and 102 s^{-1}. As pointed out above, at low $\dot{\gamma}$ values only the longer chains having long relaxation times will be oriented, with a low cutoff end at the critical orientation *M** value (line 1 in Figure 12). As $\dot{\gamma}$ is increased, the population of polymer molecules with lower molecular weights (lower relaxation times) also become extended, thus increasingly "cutting into" the distribution from the high molecular tail downward (line 2 in Figure 12).

In practice, this process cannot continue indefinitely. In fact, the relaxation time for the shortest chains is short and cannot form long-lived extended structures. Thus, there is a limiting value for the critical orientation molecular weight below which the stable oriented structures cannot be formed even at high values of shear rates. It should be noted that the *K* and α parameters in eq 4 have been calculated for the step shear condition in which the strain (1428%) was kept constant. Both the total strain and the shear rate affect the coil to stretch transition in a shear flow field. Further experimental results are required to understand the effect of

the total strain. Calculated values of the parameters K, α, and M^* are based on three experimental data points and therefore must be used with caution.

Conclusions

1. The SAXS patterns of isotactic polypropylene melt at 140 °C show the development of oriented crystalline lamellae upon application of step shear at 1428% strain and shear rates of 10, 57, and 102 s^{-1}. Results suggest that the shear induces orientation and alignment of chain segments of i-PP molecules in the flow direction. A cluster of aligned chain segments may initiate primary nuclei, from which the oriented crystals (kebab) grow in perpendicular direction by the process of secondary nucleation after the cessation of flow.

2. Because of the imposed step shear, the crystallization kinetics of (both oriented and unoriented species) i-PP increases by 2 orders of magnitude compared to quiescent crystallization. The increase in crystallization rate is mainly due to the orientation-induced primary nuclei. The unoriented crystallites are related to the formation of β-form crystals.

3. The fraction of oriented crystallites in the polypropylene bulk is lower at a shear rate of 10 s^{-1} compared to the oriented fraction at shear rates of 57 and 102 s^{-1}.

4. No significant difference in the oriented fraction was observed at shear rates of 57 and 102 s^{-1}. This "unexpected" observation can be explained by the concept of critical orientation molecular weight (M^*), which was first proposed by Keller. Under the imposed shear flow conditions, only polymer molecules having a molecular weight above a critical orientation molecular weight can form oriented structures.

5. In analogy with Keller's observations in dilute systems, the relationship between the critical orientation molecular weight and shear rate (at constant strain) (M^* vs $\dot{\gamma}^{-\alpha}$) has been used to calculate the value of the exponent α from the critical orientation molecular weight values at different shear rates. The value of α for i-PP in the chosen experimental conditions is 0.15.

6. The critical orientation molecular weight is a very sensitive quantity at low shear rates and reaches a plateau above a shear rate of 60 s^{-1}. The value of M^* for high shear rates is about 300 000 g/mol. At shear rates of 57 and 102 s^{-1}, the value for the fraction of oriented material does not vary significantly.

7. The step shear experiment using the modified Linkam shear stage provides a technique in which both the shear rate and the shear strain can be varied independently.

Acknowledgment. We record our appreciation to the late Prof. Andrew Keller and to Profs. Richard S. Stein, J. Kornfield, and H. Janeschitz-Kriegl for helpful discussions and interpretations of the results. The experimental assistance by Drs. Dufei Fang, Lizhi Liu, Weidong Liu, Shaofeng Ran, Fengji Yeh, and Steven Zong at Stony Brook is greatly appreciated. We express our thanks to the US−Spain Science & Technology Program 1999 for the support of travelling for this joint research project. The financial support for this work was also provided by NSF DMR-9732653, DGICYT, Spain (Grant PB-0049), and by ExxonMobil Chemical Company.

References and Notes

(1) Lee, O.; Kamal, M. R. *Polym. Eng. Sci.* **1999**, *39*, 236.
(2) Pennings, A. J.; Van der mark, J. M. A.; Booij, H. C. *Kolloid Z. Z. Polym.* **1970**, *236*, 99.
(3) Mackley, M. R.; Keller, A. *Polymer* **1973**, *14*, 16.
(4) Pope, D. P.; Keller, A. *Colloid Polym. Sci.* **1978**, *256*, 751.
(5) Miles, M. J.; Keller, A. *Polymer* **1980**, *21*, 1295.
(6) Keller, A.; Kolnaar, H. W. H. *Mater. Sci. Technol.* **1997**, *18*, 189.
(7) Jerschow, P.; Janeschitz-Kriegl, H. *Int. Polym. Process.* **1997**, *12*, 72.
(8) Eder, G.; Janeschitz-Kriegl, H.; Liedauer, S. *Prog. Polym. Sci.* **1990**, *15*, 629.
(9) Eder, G.; Janeschitz-Kriegl, H. *Mater. Sci. Technol.* **1997**, *18*, 268.
(10) Liedauer, S.; Eder, G.; Janeschitz-Kriegl, H. *Int. Polym. Process.* **1995**, *10*, 243.
(11) Liedauer, S.; Jerschow, P.; Geymayer, W.; Ingolic, E. *Int. Polym. Process.* **1993**, *8*, 236.
(12) Kumaraswamy, G.; Issaian, A. M.; Kornfield, J. A. *Macromolecules* **1999**, *32*, 7537.
(13) Kumaraswamy, G.; Varma, R. K.; Issaian, A. M.; Kornfield, J. A.; Yeh, F.; Hsiao, B. S. *Polymer*, in press.
(14) Bayer, R. K.; Eliah, A. E.; Seferis, J. C. *Polym. Eng. Rev.* **1984**, *4*, 201.
(15) Ania, F.; Bayer, R. K.; Tschmel, A.; Michler, H. G.; Naumann, I.; Baltá Calleja, F. J. *J. Mater. Sci.* **1996**, *31*, 4199.
(16) Rueda, D. R.; Ania, F.; Baltá Calleja, F. J. *Polymer* **1997**, *38*, 2027.
(17) Haas, T. W.; Maxwell, B. *Polym. Eng. Sci.* **1969**, *9*, 225.
(18) Kobayashi, K.; Nagasawa, J. *J. Macromol. Sci., Phys. B* **1970**, *4*, 331.
(19) Wereta, A.; Gogos, C. *Polym. Eng. Sci.* **1971**, *11*, 19.
(20) Krueger, D.; Yeh, G. S. Y. *J. Appl. Phys.* **1972**, *43*, 4339.
(21) Fritzsche, A. K.; Price, F. P. *Polym. Eng. Sci.* **1974**, *14*, 401.
(22) Tan, V.; Gogos, C. *Polym. Eng. Sci.* **1971**, *11*, 512.
(23) Lagasse, R. R.; Maxwell, B. *Polym. Eng. Sci.* **1976**, *16*, 189.
(24) Fritzsche, A. K.; Price, F. P.; Ulrich, R. D. *Polym. Eng. Sci.* **1976**, *16*, 182.
(25) Ulrich, R. D.; Price, F. P. *J. Appl. Polym. Sci.* **1976**, *20*, 1077.
(26) Tribout, C.; Monasse, B.; Haudin, *Colloid Polym. Sci.* **1996**, *274*, 197.
(27) Kalay, G.; Bevis, M. J. *J. Polym. Sci., Polym. Phys.* **1997**, *35*, 265.
(28) Huang, H. *J. Appl. Polym. Sci.* **1998**, *67*, 2111.
(29) Wilkinson, A. N.; Ryan, A. J. *Polymer Processing and Structure Development*; Kluwer: Dodrecht, 1998.
(30) Varga, J. *J. Mater. Sci.* **1992**, *27*, 2557.
(31) Varga, J.; Karger-Kocsis, J. *J. Polym. Sci., Part B: Polym. Phys.* **1996**, *34*, 657.
(32) Kargin, V. A.; Andrianova, G. P. *Dokl. Akad. Nauk USSR* **1962**, *146*, 1337.
(33) Binsbergen, F. L. *Nature* **1966**, *211*, 516.
(34) Thomason, J. L.; Van Rooyen, A. A. *J. Mater. Sci.* **1992**, *27*, 897.
(35) Misra, S.; Lu, F. M.; Spruiell, J. E.; Richeson, G. C. *J. Appl. Polym. Sci.* **1995**, *56*, 1761.
(36) Vleeshouwers, S.; Meijer, H. E. H. *Rheol. Acta* **1996**, *35*, 391.
(37) Moitzi, J.; Skalicky, P. *Polymer* **1993**, *34*, 3168.
(38) Haudin, F. J.; Monasse, B. *J. Mater. Sci.* **1999**, *34*, 2089.
(39) Wunderlich, B. *Macromolecular Physics*; Academic: New York, 1973; Vol. 2.
(40) Chu, B.; Harney, P. J.; Li, Y.; Linliu, K.; Yeh, F.; Hsiao, B. S. *Rev. Sci. Instrum.* **1994**, *65*, 597.
(41) White, H. M.; Bassett, D. C. *Polymer* **1997**, *38*, 5515.
(42) Ran, S.; Zong, X.; Fang, D.; Hsiao, B.; Chu, B.; Ross, R. *J. Appl. Crystallogr.*, in press.
(43) Goschel, U.; Swartjes, F. H. M.; Peters, G. W. M.; Meijer, H. E. H. *Polymer* **2000**, *41*, 1541.
(44) Lotz, B.; Wittmann, J. C. *J. Polym. Sci.* **1986**, *24*, 1541.
(45) Verma, R. K.; Hsiao, B. S. *Trends Polym. Sci.* **1996**, *4*, 312.

MA001124Z